Supporting information

Sirtuin Deacetylation Mechanism and Catalytic Role of the Dynamic Cofactor Binding Loop

Yawei Shi[1], Yanzi Zhou[1,2], Shenglong Wang[1], and Yingkai Zhang[1,*]

[1]Department of Chemistry, New York University, New York, New York

[2] Institute of Theoretical and Computational Chemistry, Key Laboratory of Mesoscopic Chemistry, School of Chemistry and Chemical Engineering, Nanjing University, Nanjing 210093, P.R. China

Table of Contents

I. Figures S1-S8

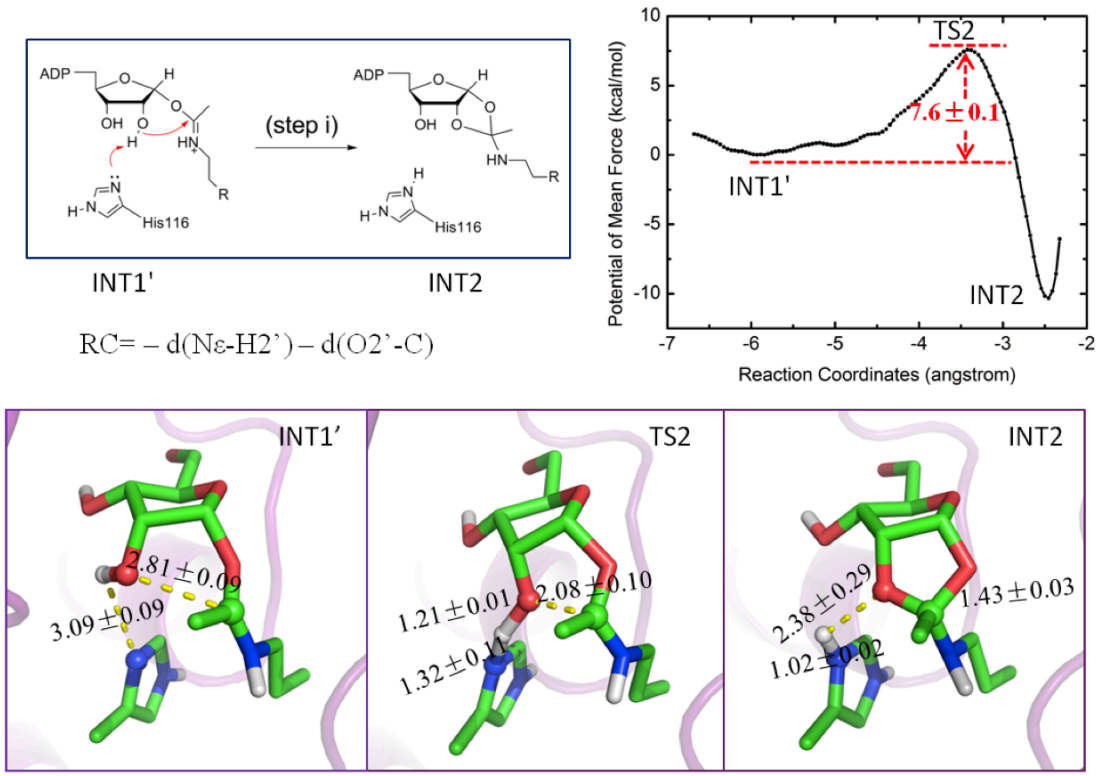

Figure S1. **Step i in the second stage of the deacetylation reaction catalyzed by Sir2Tm.**
Reaction mechanism and chosen reaction coordinate (top left), free energy profile (top right) and critical structures (bottom).

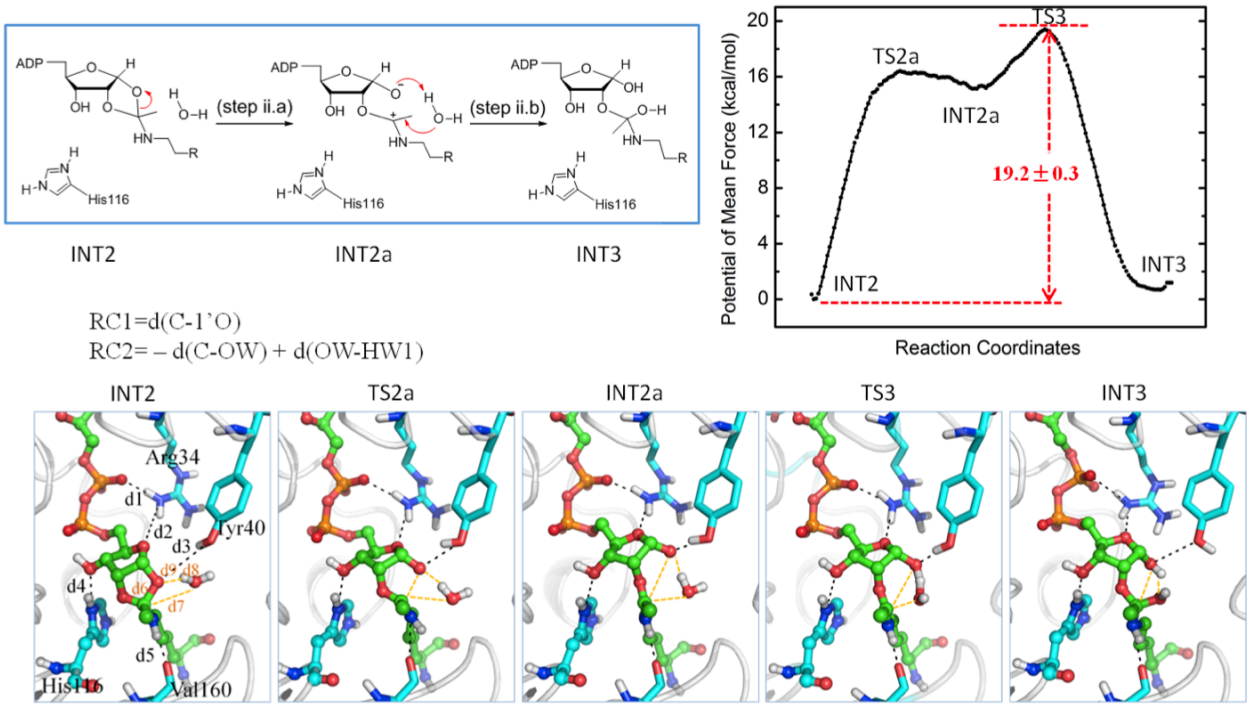

Critical bond	distance(Å)	INT2	TS2a	INT2a	TS3	INT3
d1	NH1(Arg34)-OPA1(SUB)	2.82±0.08	2.79±0.09	2.82±0.08	2.84±0.08	2.81±0.07
d2	NH1(Arg34)-O'N4(SUB)	4.21±0.11	2.82±0.08	2.78±0.08	2.8±0.08	2.81±0.08
d3	OH(Tyr40)-O1'(SUB)	4.01±0.21	2.74±0.1	2.68±0.11	2.71±0.12	3.58±0.15
d4	ND1(His116)-O'N3(SUB)	2.74±0.09	2.8±0.09	2.87±0.08	2.87±0.06	2.86±0.07
d5	O(Val160)-N(SUB)	2.84±0.07	2.77±0.08	2.79±0.07	2.8±0.08	2.84±0.07
d6	C(SUB)-O1'(SUB)	1.46±0.02	2.51±0.02	3.32±0.06	3.40±0.12	3.42±0.10
d7	C(SUB)-OW(WAT)	3.98±0.25	3.58±0.54	2.53±0.04	2.05±0.07	1.46±0.03
d8	OW(WAT)-HW1(WAT)	0.98±0.02	1.00±0.03	1.01±0.03	1.20±0.06	1.95±0.04
d9	O1' (SUB)-HW1(WAT)	1.97±0.26	1.80±0.06	1.71±0.02	1.23±0.08	0.98±0.01

Figure S2. **Step ii in the second stage of the deacetylation reaction catalyzed by Sir2Tm.**
Reaction mechanism and chosen reaction coordinate (top left), free energy profile (top right) and critical structures (bottom). Step ii employs a stepwise mechanism including step a and b.

Hydrogen bond network between Sir2Tm active site residues and the substrate (SUB) involved in the step ii are labeled in black (d1-d5), the critical bonds (d6-d9) involved in the reaction are labeled in orange and all the distances are presented in the table. The average value and statistic error are show. The states where h-bond is not formed are highlighted in red. It is indicated that Tyr40 dose not form hydrogen bond with the substrate 1'O atom at INT2 and INT3 state, but the indicated hbond is observed at the transition state of step ii, which shed lights on to the catalytic function of Tyr40 for the reaction. Similar function has been found for Arg34.

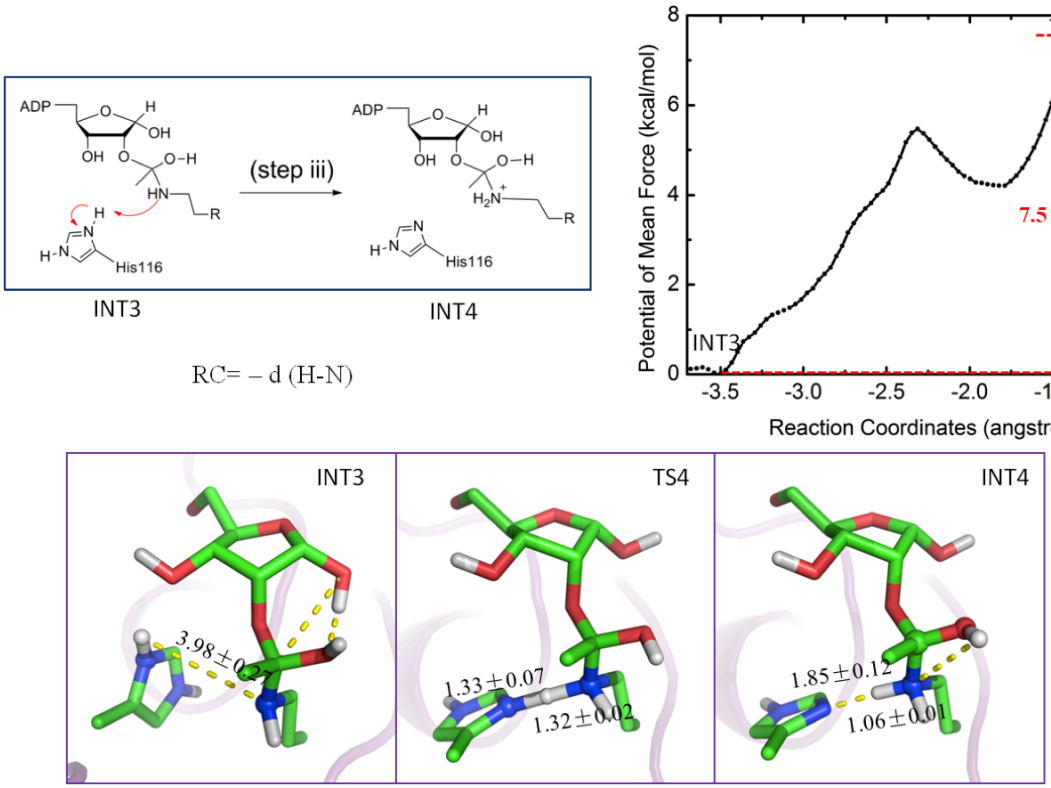

Figure S3. **Step iii in the second stage of the deacetylation reaction catalyzed by Sir2Tm.**
Reaction mechanism and chosen reaction coordinate (top left), free energy profile (top right) and critical structures (bottom).

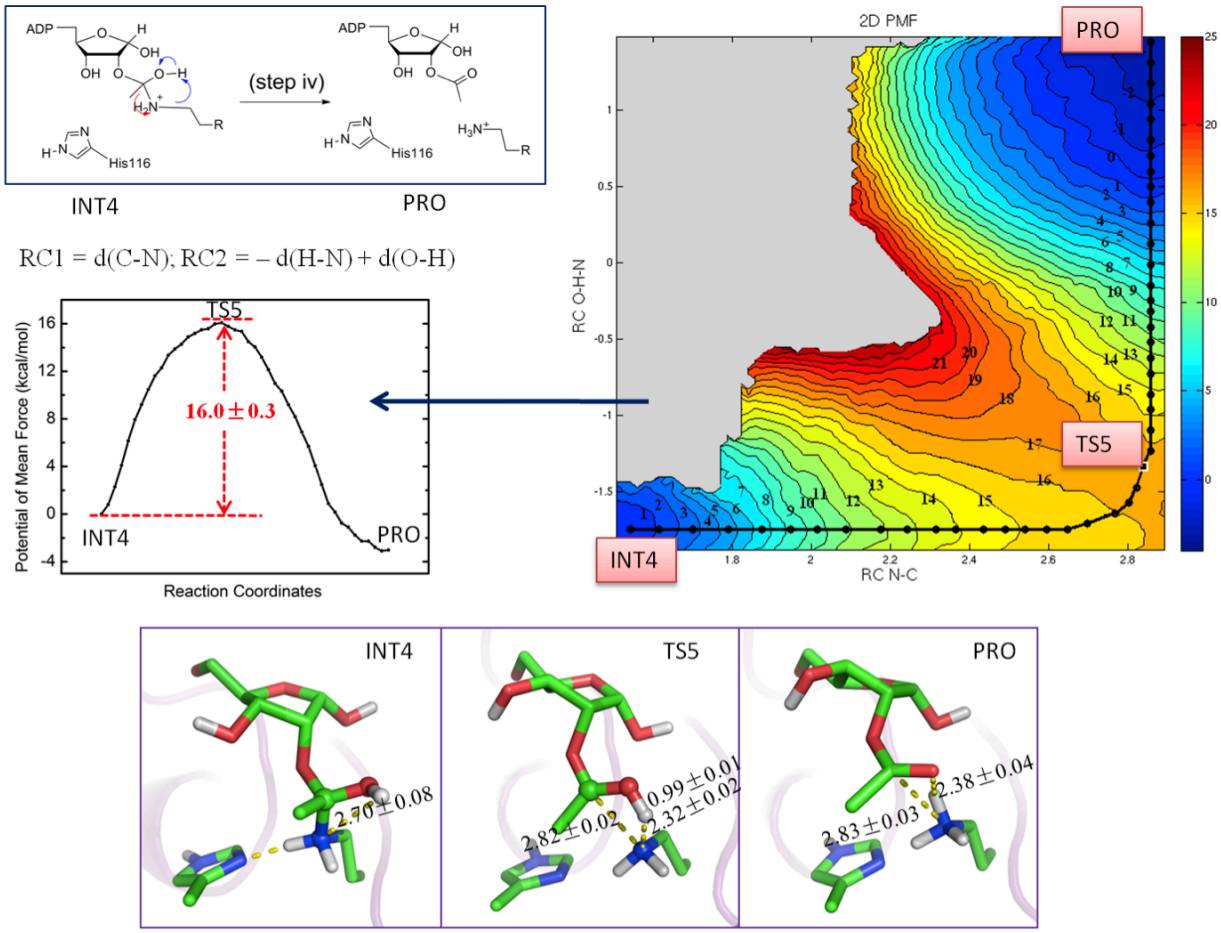

Figure S4. **Step iv in the second stage of the deacetylation reaction catalyzed by Sir2Tm.**
Reaction mechanism and chosen reaction coordinate (top left), free energy profile (top right) and critical structures (bottom). The two-dimensional free energy surface is mapped to one dimensional free energy profile (top left) and the free energy barrier is determined. The two-dimensional reaction coordinate is also illustrated.

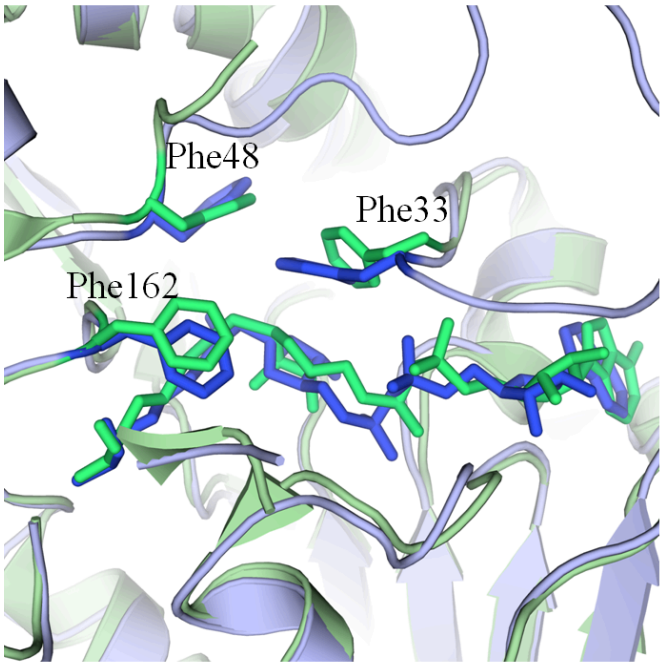

Figure S5. Superimposition of the active sites of Sir2Tm–S–alkylamidate intermediate complex crystal structure (PDB code 3D81, green) and the snapshot of 20 ns MD simulation of INT1' (blue). The cluster of phenylalanine side chains, Phe33, Phe48, and Phe162, are highlighted.

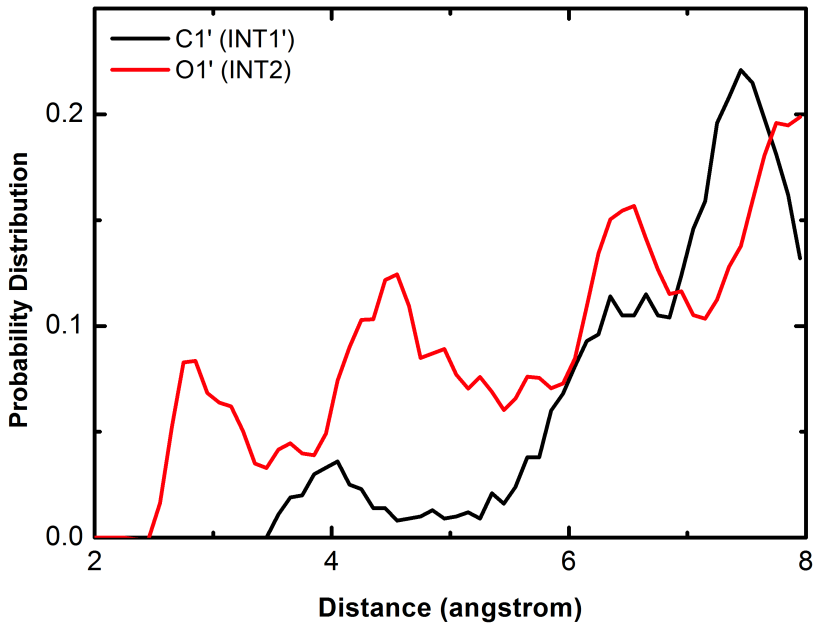

Figure S6. Radial distribution of water in the active site showing different degree of water occupancy. The water probability distribution is calculated within 8 Å of the reaction center, C1' atom for INT1' and O1' for INT2, respectively.

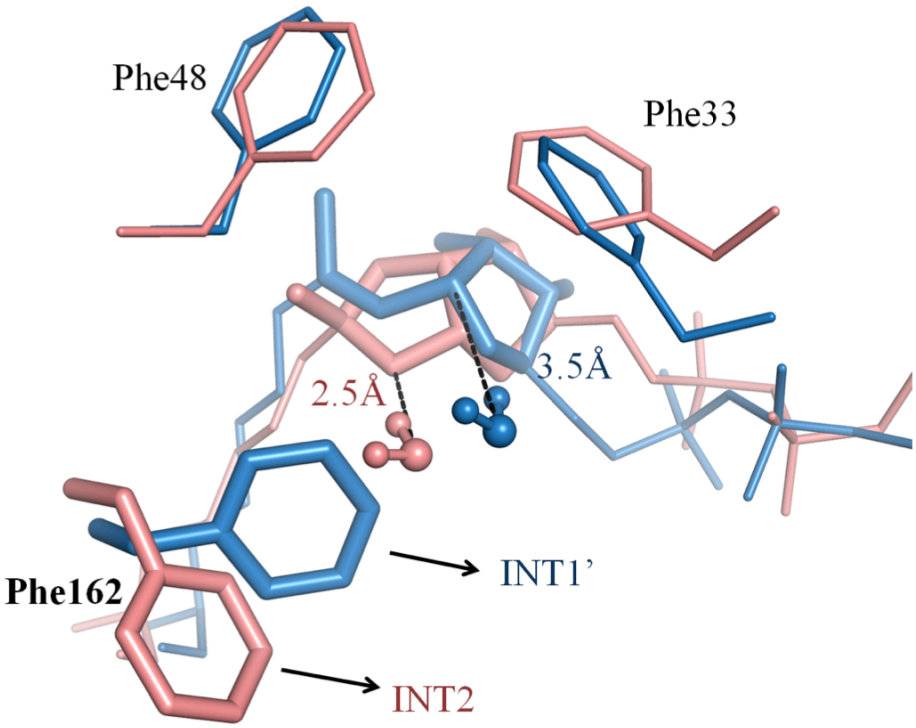

Figure S7. Superimposition of INT1' and INT2 showing the different placement of the important Phenylalanine cluster (Blue: INT1'; Pink: INT2). The water which is nearest to the intermediate N-ribose or the bicyclic ring is shown, the minimum distance from the oxygen atom of water to the reaction center (C1'atom in INT1', O1' atom in INT2) of the intermediate is indicated.

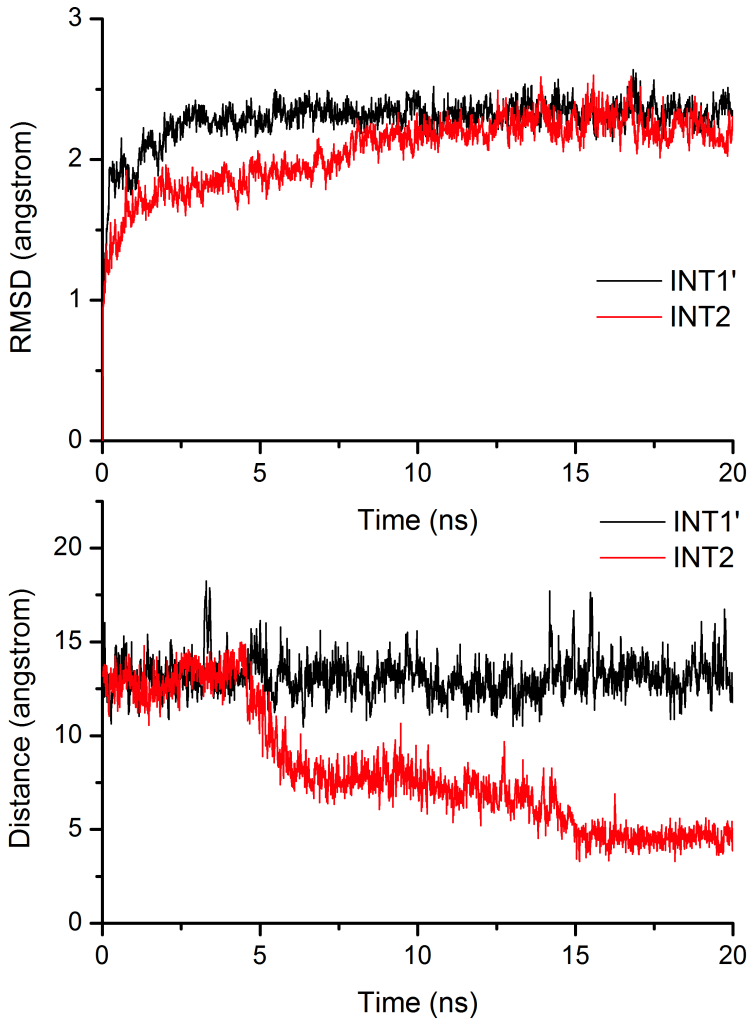

Figure S8. RMSD and trajectory analysis of the classical MD simulations at INT1' state (black) and INT2 state (red). Top: Time dependent RMS deviations of Sir2Tm protein heavy atoms during 20 ns MD simulations. Bottom: Time dependent trajectories of the critical distance of OH(Tyr40)-O1'(SUB) during 20 ns MD simulations.

II. Complete Citation for Reference 34, 50, 51

(34) Shao, Y.; Fusti-Molnar, L.; Jung, Y.; Kussmann, J.; Ochsenfeld, C.; Brown, S. T.; Gilbert, A. T. B.; Slipchenko, L. V.;Levchenko, S. V.; O'Neill, D. P.; Distasio, Jr.,R. A.; Lochan, R. C.; Wang, T., Beran, G. J. O.; Besley, N. A.; Herbert, J. M.;Lin, C. Y.;Voorhis, T. V.; Chien, S. H.; Sodt, A.; Steele, R. P.; Rassolov, V. A.; Maslen, P. E.; Korambath, P. P.; Adamson, R. D.; Austin,B.; Baker, J.; Byrd, E. F. C.; Dachsel, H.; Doerksen, R. J.; Dreuw, A.; Dunietz, B. D.; Dutoi, A. D.; Furlani, T. R.; Gwaltney, S. R.; Heyden, A.; Hirata, S.; Hsu, C. P.; Kedziora, G.; Khalliulin, R.Z.; Klunzinger, P.; Lee, A. M.; Lee, M. S.; Liang, W.; Lotan, I.; Nair, N.; Peters, B.;Proynov, E. I.; Pieniazek, P. A.; Rhee, Y. M.; Ritchie, J.; Rosta, E.; Sherrill, C. D.; Simmonett, A. C.; Subotnik, J. E.; Woodcock, III, H. L.; Zhang, W.; Bell, A. T.; Chakraborty, A. K.; Chipman, D. M.; Keil, F. J.; Warshel, A.; Hehre, W. J.; Schaefer, III, H. F.;Kong, J.;Krylov, A. I.;Gill, P. M. W.; Head-Gordon, M. Advances in Methods and Algorithms in a Modern Quantum Chemistry Program Package. *Phys. Chem. Chem. Phys.* **2006**, *8*, 3172-3191.

(50) Schuetz, A.; Min, J.; Antoshenko, T.; Wang, C.L.; Allali-Hassani, A.; Dong, A.; Loppnau, P.; Vedadi, M.; Bochkarev, A.; Sternglanz, R.; Plotnikov, A. N. Structural Basis of Inhibition of the Human NAD+-dependent Deacetylase SIRT5 by Suramin. *Structure* **2007**, *15*, 377-389.

(51) Jin, L.; Wei, W. T.; Jiang, Y. B.; Peng, H.; Cai, J. H.; Mao, C.; Dai, H.; Choy, W.; Bemis, J. E.; Jirousek, M. R.; Milne, J. C.; Westphal, C. H.; Perni, R. B. Crystal Structures of Human SIRT3 Displaying Substrate-induced Conformational Changes. *J. Biol. Chem.* **2009**, *284*, 24394-24405.

III. Computational Details

Our overall enzyme reaction simulation protocol is illustrated in Figure S9.

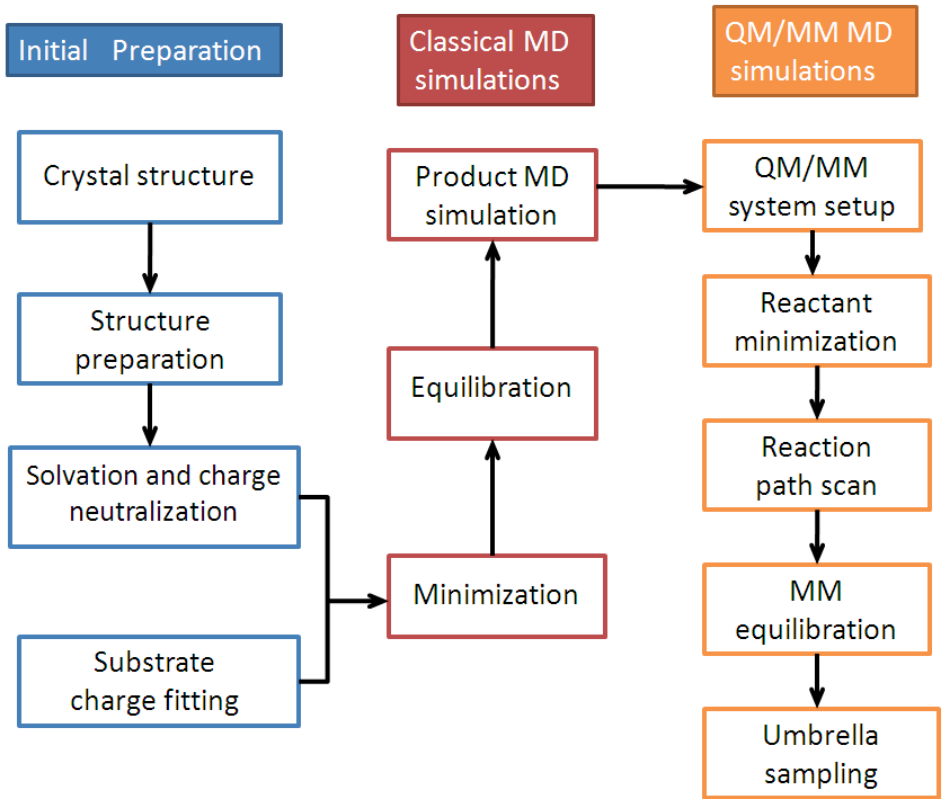

Figure S9. Flow chart of our computational protocol.

The initial Sir2Tm-alkylamidate enzyme complex was prepared based on the crystal structure of 3D81,[1] the first reported crystal structure of Sir2 with the S-alkylamidate intermediate bound in the active site, and modification was made to convert the sulfur atom to oxygen. The protonation states of charged residues were determined at constant pH 7 based on pKa calculations via the program PROPKA[2] and the consideration of the local hydrogen bonding network. The whole system was then solvated into a ~60×60×84 A^3 TIP3P water rectangular box with a 10 Å buffer distance between the solvent box wall and the nearest solute atom. Seven sodium ions were added to neutralize the system charge. Finally, the whole simulation system had 30953 atoms. After a series of minimizations and equilibrations, standard molecular dynamics simulations with periodic boundary condition were carried out for more than 20 ns. The trajectory was stabilized after 3 ns (see RMSD result in Figure S8), and a snapshot at the 10 ns simulation time has been employed for subsequent QM/MM simulations. In the MD simulations, long-range electrostatic interactions were treated with particle mash Ewald (PME) method[3,4] and 12Å cutoff was used for both van der Waals interactions and PME in real space. The pressure was coupled every 1 ps with isotropic position scaling and maintained at 1 atm. The Newton equations of motion were integrated with velocity Verlet algorithm. The shake algorithm[5] was applied to constrain all bonds involving hydrogen atoms with tolerance of 10^{-5}Å. A time step of 2 fs was used, and Berendsen thermostat method[6] has been used to control the system temperature at 300 K. All MD simulations were preformed with Amber10 molecular dynamics

package,[7] employing the Amber99-SB[8-10] force field for the protein and the TIP3P model[11] for water molecules. Force field parameters for O-alkylamidate were developed based on the parameters of NAD^+ from Ryde[12] and generated from AMBER GAFF force field via AMBER tools[13], partial charges of the novel peptidyl imidate moiety were fitted with HF/6-31G(d) calculations and the RESP module in the Amber package (Figure S10).

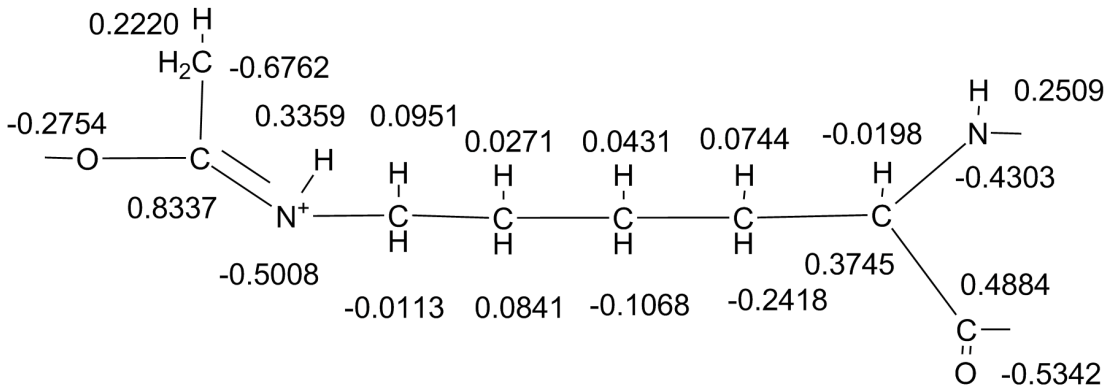

Figure S10. Structure representation and partial charge of the peptidyl imidate moiety of O-alkylamidate intermediate, generated with HF/6-31G(d) calculations and the RESP module in the Amber package. The equivalent hydrogen atoms with the same charge are only shown by one representation.

With the snapshot taken from the MD trajectory, the QM/MM model was prepared by deleting the solvent molecules beyond 30 Å from the reaction center (O_2' of N-ribose). The resulted system had 12301 atoms. Our choice of the QM sub-system is based on proposed reaction schemes, and includes fragments directly participating in the reaction. The defined QM subsystems had 62 atoms, as shown in Figure S11, including the moiety of His116, the ribose ring and di-phosphate group portions of NAD+ as well as the peptidyl imidate, treated by B3LYP functional with 6-31G(d) basis set. The QM/MM boundary atoms were treated with the improved pseudobond approach.[14,15] All other atoms were described by Amber99SB molecular mechanical force field and the TIP3P model for water molecules. The spherical boundary condition was applied and the atoms 22Å beyond sphere centered on 2'O of N-ribose were fixed. The 18 and 12 Å cutoffs were employed for electrostatic and van der Waals interactions, respectively. There was no cutoff for electrostatic interactions between QM and MM regions. The prepared system was first minimized by QM/MM optimization. Then, 30ps *ab initio* QM/MM MD simulations were carried out (see next paragraph for details) with the time step 1 fs and the Beeman algorithm[16] to integrate the Newton equations of motion, as well as the Berendsen thermostat method to control the system temperature at 300 K. All *ab initio* QM/MM calculations were performed in modified Q-Chem[17] and Tinker[18] programs.

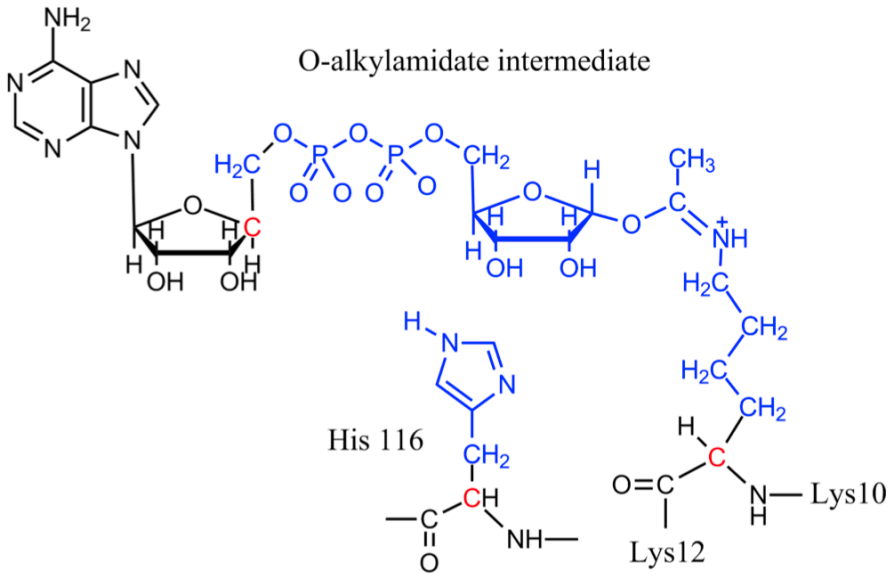

Figure S11. Illustration of the QM/MM partition for **step i**. Color notations: black, MM subsystem; red, boundary carbon atoms in the QM subsystem described by improved pseudobond parameters; blue, all other atoms in the QM subsystem.

To study the mechanism of step i in the second stage of the deacetylation reaction, we employed the sum of two bond lengths, Nε-H_2' and O_2'-C as the reaction coordinate: RC = – $d_{Nε\text{-}H2'}$ – $d_{O2'\text{-}C}$, and used an iterative minimization procedure with the reaction coordinate driving method[19] to first map out the minimum energy path (MEP) associated with the reaction coordinate. For each determined structure along the reaction path, the MM subsystem was further equilibrated with 500 ps molecular mechanical MD simulation. Then the resulting snapshot was used as the starting structure for *ab initio* QM/MM MD simulations with umbrella sampling. Each window was simulated for 30 ps. The configurations after 10 ps for each window were collected for data analysis. The probability distributions along the reaction coordinate were determined for each window and pieced together with the WHAM[20,21] to calculate the free energy profile along the reaction coordinate. This computational protocol has successfully been applied to study several enzymes as well as chemical reactions in aqueous solution[22-29].

With the computationally determined bicyclic intermediate, first we carried out QM/MM calculations to examine several potential reaction schemes without involving a water molecule acting as a nucleophile for the initial step, which all yielded high energy barriers of more than 40 kcal/mol. (See section IV "Examination of other reaction schemes" for details). These failed attempts indicate that the bicyclic collapse step could not proceed without the initial participation of water, meanwhile, quite some experimental studies[30,31] have indicated that a water molecule will be needed to act as nucleophile to attack the proposed bicyclic intermediate to yield the final product. Thus we resolvated the QM/MM determined bicyclic intermediate with a rectangular water box, and carried out 20 ns classical MD simulations with periodic boundary condition (see RMSD result in Figure S8). Force field parameters for bicyclic intermediate were developed based on the parameters of NAD^+ from Ryde[12] and generated from AMBER GAFF force field via AMBER tools[13], partial charges of the novel bicyclic ring and peptidyl imidate moiety were fitted with HF/6-31G(d) calculations and the RESP module in the Amber package (Figure S12). One very interesting finding is that during the

classical MD simulation of the bicyclic intermediate, one water molecule comes into the active site through a water channel close to the dynamic cofactor binding loop and is positioned at a geometrically favored place to form a stable hydrogen bond with 1'O atom of the intermediate. With the snapshot taken at 20 ns of the trajectory, a new QM/MM system was prepared, in which the water molecule was included into the new QM sub-system containing 65 atoms (Figure S13). Then by choosing appropriate reaction coordinates, free energy profiles for the step ii, iii and iv were determined sequentially with reaction path/surface scan, MM equilibration and B3LYP/6-31G(d) QM/MM MD simulations with umbrella sampling following the same protocol as for the first step.

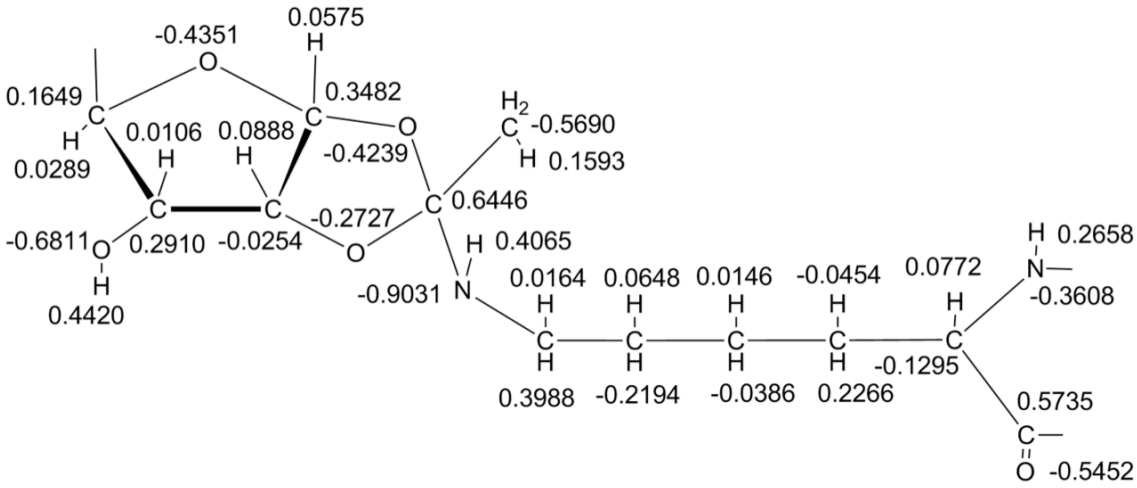

Figure S12. Structure representation and partial charge of the bicyclic ring and peptidyl imidate moiety of bicyclic intermediate, generated with HF/6-31G(d) calculations and the RESP module in the Amber package. The equivalent hydrogen atoms with the same charge are only shown by one representation

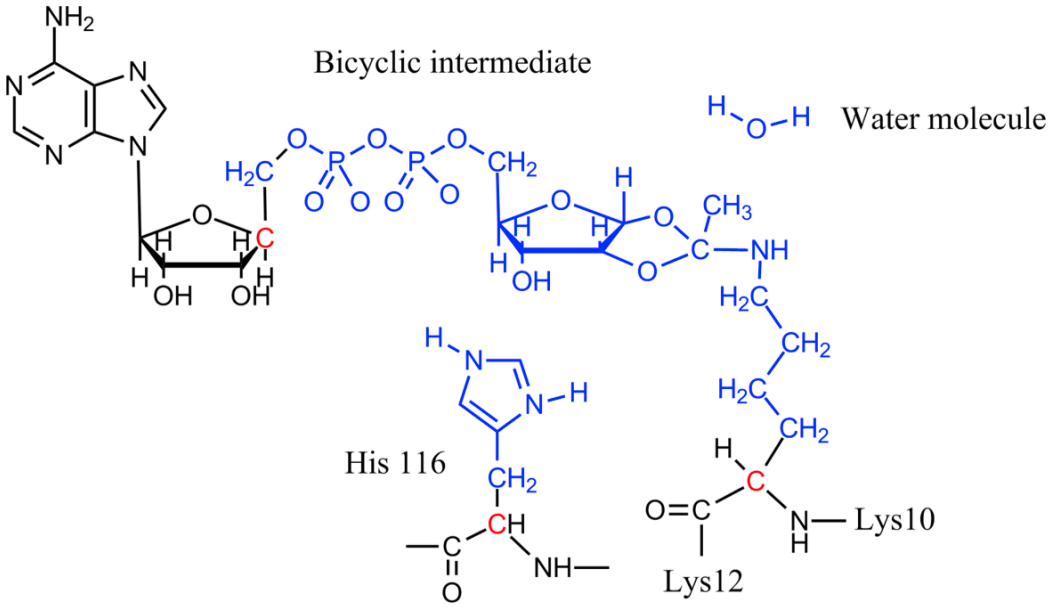

Figure S13. Illustration of the QM/MM partition for **step ii-iv**. Color notations: black, MM subsystem; red, boundary carbon atoms in the QM subsystem described by improved pseudobond parameters; blue, all other atoms in the QM subsystem.

IV. Examination of other reaction schemes

Besides our computationally characterized reaction mechanism as shown in Figure1, 2, S1-S4, we have used *ab initio* QM/MM calculations to examine previously suggested alternative reaction schemes[32] as shown in Figure S14 as well as other potential mechanisms, and have explored choices of different reaction coordinates. Below we summarize our attempts for each reaction step in the second stage of Sir2Tm catalyzed deacetylation reaction.

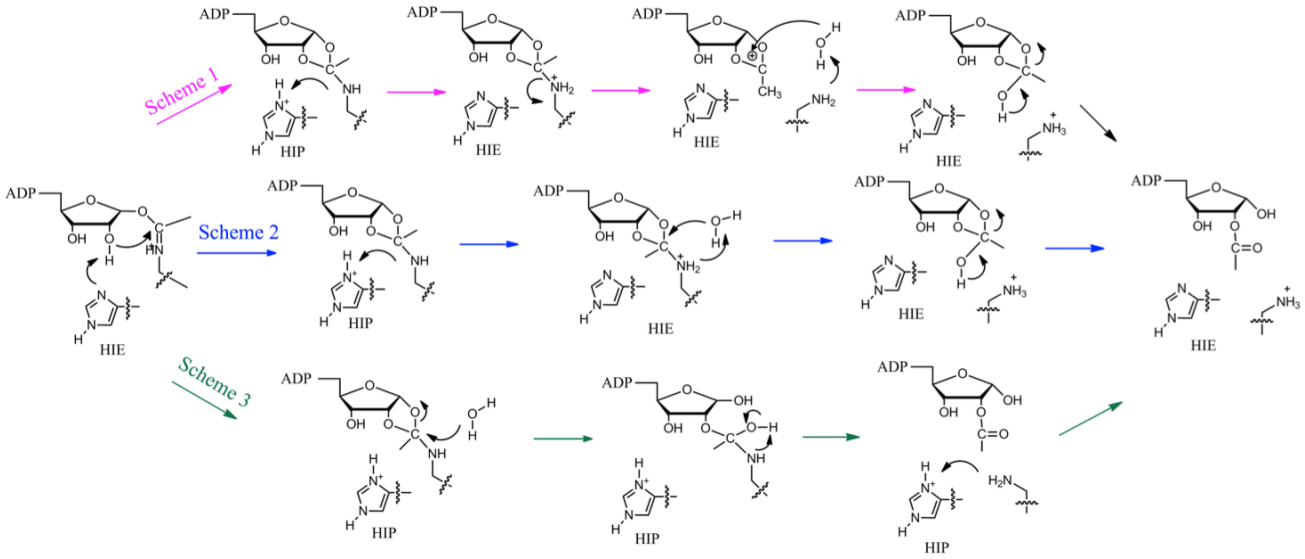

Figure S14. Summary of some previously suggested alternative reaction schemes

4.1. Step i.

For step i in the second stage of the deacetylation reaction, our computationally characterized reaction scheme (Figure 1, S1) is the same as the one previously suggested, as shown in Figure S14. In addition, we have examined a substrate-assisted reaction pathway, in which the phosphate moiety serves as the base, as shown in Figure S15. The calculated potential energy reaction barrier for this reaction scheme is 25.9 kcal/mol, which is significantly higher than that of the employment of His116 as the base but still reasonable. Thus we speculate that this might be one probable reaction pathway for the His116A mutant deacetylation reaction. Meanwhile, previously His116 has also been suggested to deprotonate the 2' OH group through a 3' OH shuttling mechanism. However, the Sir2Tm S-alkylamidate complex crystal structure as well as our MD simulations results demonstrated that His116 is in contact with the N-ribose 2'OH so that it can directly serve as a base.

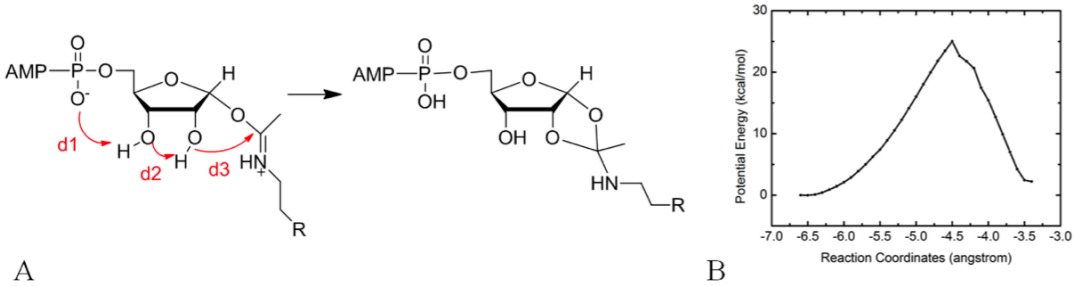

Figure S15. An intramolecular mechanism in which the phosphate moiety of the intermediate could deprotonate the 2' OH group through a shuttling mechanism. This always resulted in a higher energy profile than our proposed mechanism but may be the mechanism for sirtuins H116A mutant deacetylation. (A) The mechanism scheme. d1 and d2 indicate the forming O-H bond, d3 indicates the forming O-C bond. (B) Potential energy profile for the shuttling mechanism. The reaction coordinates are RC= –d1(O_P-H_{O3}) – d2(O_3-H_{O2}) – d3(O_2-C).

4.2. Step ii.

Step ii in the second stage of the deacetylation reaction, as known to all, is the most mysterious part of the deacetylation reaction. With the QM/MM determined bicyclic intermediate, first we examined one previously suggested reaction pathway without the initial participation of a water molecule (scheme 1 in Figure S14). Considering that the proton transfer and C-N bond breaking can happen either stepwisely or concertedly, both possibilities have been tested, which lead to potential energy barriers higher than 40 kcal/mol, as shown Figure S16 and S17.

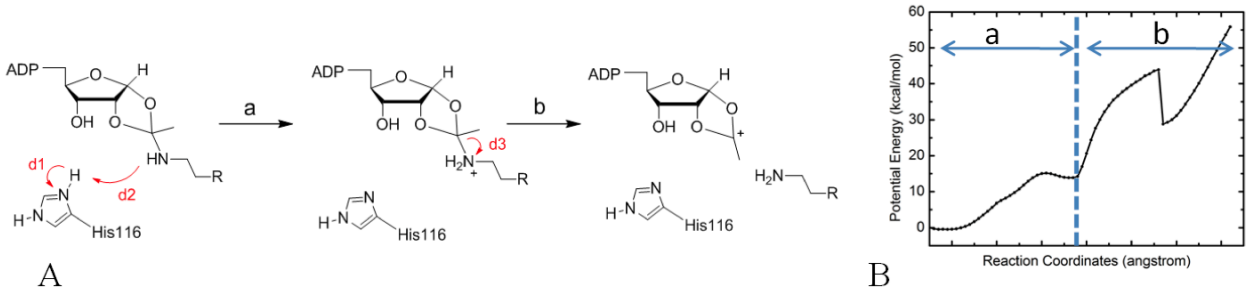

Figure S16. A stepwise mechanism in which the protonated side chain of the His116 first acts as a general acid to reprotonate the imino group (-NH) and then the C-N bond breaks. This always resulted in a reasonable energy barrier for *step a*while following by uphill energy profiles with unstable intermediate for *step b*. (A) The mechanism scheme. d1 indicates the breaking N-H bond, d2 indicates the forming N-H bond, d3 indicates the breaking N-C bond. (B) Potential energy profile for the stepwise mechanism. The reaction coordinates are step a: RC= d1(N_{His}-H)– d2(N-H); step b: RC=d3(C-N).

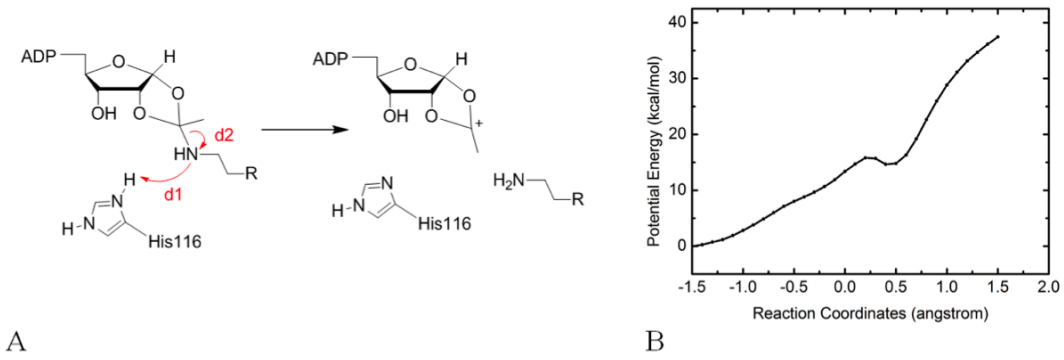

Figure S17. A concerted mechanism in which delocalized carbocation is formed from the cleavage of the indicated C–N bond, with the simultaneous reprotonation of the imino group. This always resulted in an uphill energy profile and produced an unstable intermediate that upon a short unrestrained QM/MM-MD simulation relaxed back to the bicyclic intermediate structure. (A) The mechanism scheme. d1 indicates the forming N-H bond, d2 indicates the breaking N-C bond. (B) Potential energy profile for the concerted mechanism. The reaction coordinates are RC= –d1(N-H)+d2(C-N).

The above failed attempts indicate that the bicyclic collapse step could not proceed without the participation of water, meanwhile, numerous experimental studies have indicated that a water molecule will be needed to act as nucleophile to attack the proposed bicyclic intermediate to yield the final product. Since the position and orientation of the water molecular is critical for the following reaction, the initial structure for simulating the next step of reaction (step ii) was prepared by extensive classical MD simulation, based on the computationally determined bicyclic intermediate.

The molecular dynamics simulations on enzyme-intermediate complex were carried out for more than 20 ns. One very interesting finding is that during the classical MD simulation of the bicyclic intermediate, one water molecule comes into the active site through a water channel close to the dynamic cofactor binding loop and is positioned at a geometrically favored place to form a stable hydrogen bond with 1'O atom of the intermediate. With the snapshot taken at 20 ns of the trajectory, a new QM/MM system was set up following the same protocol as before and the water molecule was included into the new QM system including 65 atoms (Figure S13). With the newly prepared QM/MM system, first we examined several different mechanistic paths for step ii in which the water directly attack the indicated C-N bond including scheme 2 in Figure 14, by exploring several different reaction coordinates. All these tests lead to very high potential energy reaction barriers (> 50 kcal/mol). Some representative results are shown in Figure S18-S20.

(1)

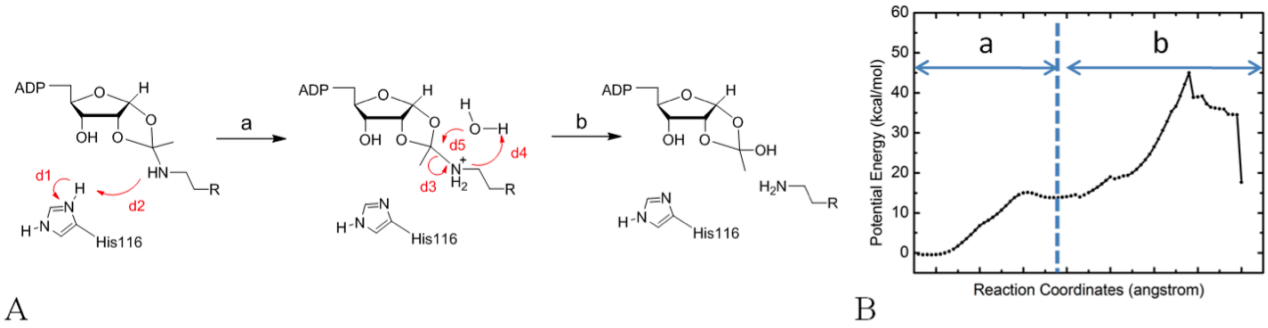

Figure S18. A SN2-like mechanism in which the nucleophile water attacks the proposed bicyclic intermediate with the concerted cleavage of the indicated C–N bond leading to the generation of the deacetylated product and the hemi-orthoester intermediate. This mechanism provided energy barrier higher than 40 kcal/mol, which is not reasonable according to the transition state theory. (A) The mechanism scheme. (B) Potential energy profile for the the SN2-like mechanism. The reaction coordinates are step a: RC= d1(N_{His}-H)–d2(N-H); step b: RC=d3(C-N)–d4(N-H_W) –d5(O_W-C).

(2)

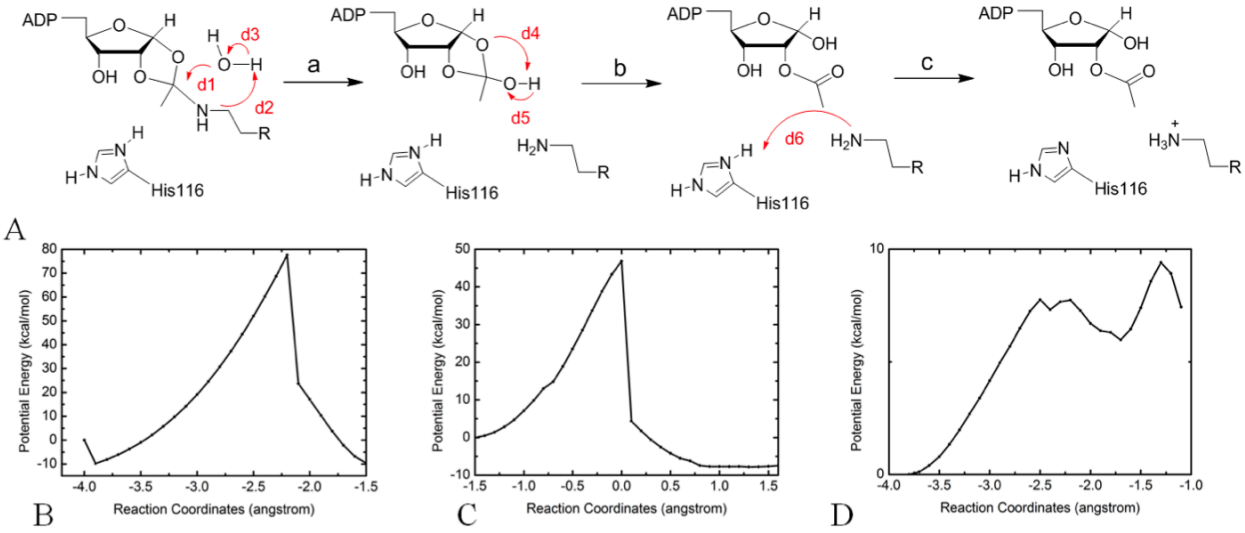

Figure S19. A mechanism in which the nucleophile water attacks the proposed bicyclic intermediate first, generating deacetylated product and hemi-orthoester intermediate, followed by a intramolecular reaction to yield the 2'OAADPR, finally with the reprotonation of the deacetylated amino group. The process of the reaction has to overcome a very high energy barrier first (>70kcal/mol), which may be caused by the steric crash in the active site when the water was driven near to the C-N bond. (A) The mechanism scheme. (B) Potential energy profile for *step a* of the mechanism. The reaction coordinates are RC= –d1(O_W-C)–d2(H_W-N)+d3(H_W-O_W). (C) Potential energy profile for *step b* of the mechanism. The reaction coordinates are RC = –d4(HW-1'O) +d5 (HW-OW). (D) Potential energy profile for *step c* of the mechanism. The reaction coordinates are RC =–d6(H-N).

(3)

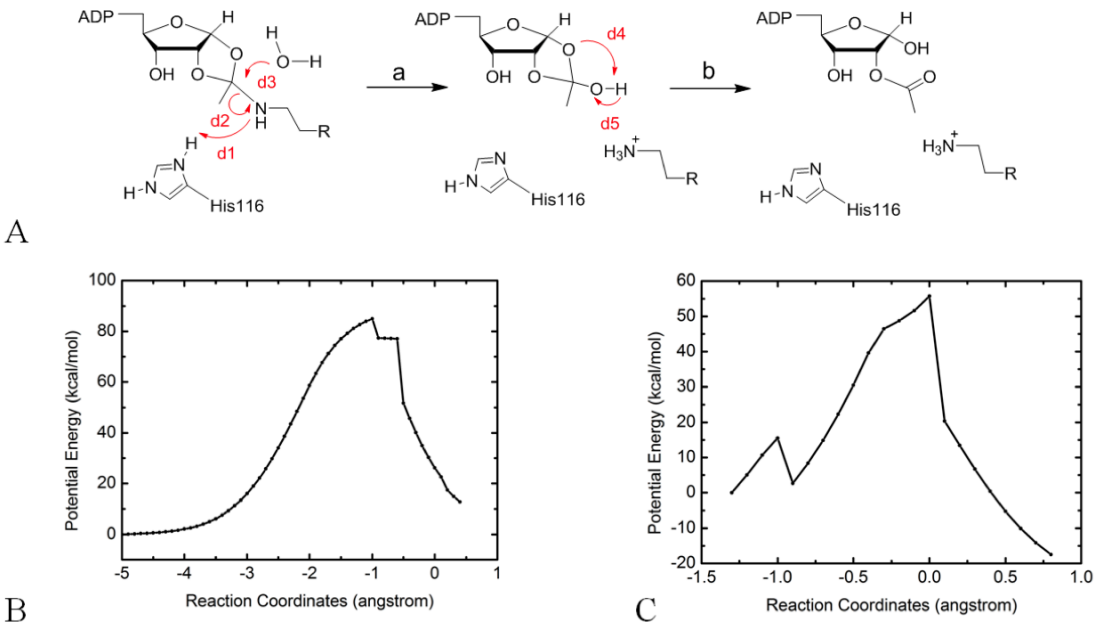

Figure S20. A SN2-like mechanism in which the nucleophile water attacks the proposed bicyclic intermediate with the concerted cleavage of the indicated C–N bond leading to the generation of the deacetylated product and the same hemi-orthoester intermediate, aided by the general acid His116 to reprotonate the imino group. This

mechanism provided higher energy barrier than normal (>50 kcal/mol) for both step a and b. (A) The mechanism scheme. (B) Potential energy profile for *step a* of the SN2-like mechanism. The reaction coordinates are RC= –d1(H-N)+d2(C-N)–d3(C-O_W). (C) Potential energy profile for *step b* of the SN2-like mechanism. RC== –d4(H_W-1'O) +d5(H_W-O_W).

Then by choosing different reaction coordinates, we tested both concerted and stepwise reaction mechanisms to form the distinct tetrahedral intermediate, which involves the cleavage of the C–O1' bond and the nucleophilic attack of the water. The concerted reaction pathway (scheme 3 in Figure S14) still leads to a high energy barrier, as shown in Figure S21. The stepwise mechanism was shown to be the most reasonable one with smooth potential energy profile and activation energy barrier consistent with the experimental value, as shown in Figure S2.

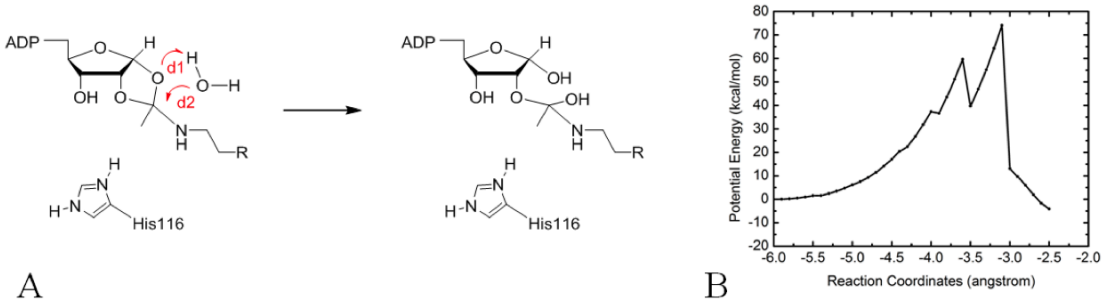

Figure S21. A concerted mechanism in which the indicated C–O1'bond is cleaved simultaneously with the attack of the water molecule and forming of new O-C bond. This mechanism produced a stable tetrahedral intermediate however with a high energy barrier (>70 kcal/mol), thus hardly seems to be the optimal reaction mechanism. (A) The mechanism scheme. d1 indicates the forming O-H bond, d2 indicates the forming O-C bond. (B) Potential energy profile for the concerted mechanism. The reaction coordinates are RC= –d1(1'O-HW)–d2(C-OW).

4.3. Step iii and iv.

After the collapse of the bicyclic ring, the following reaction mechanism becomes relatively more straightforward: the generated tetrahedral intermediate is reprotonated by His116 (step iii) which is followed by the cleavage of the indicated C–N bond and the release of the deacetylated product and 2'OAADPR (step iv). However, during the process of determining the free energy barrier for step iv, we found that the employment of one dimensional reaction coordinate is not sufficient. Thus we determined two dimensional free energy surface for step iv as shown in Figure S4.

References

(1) Hawse, W. F.; Hoff, K. G.; Fatkins, D. G.; Daines, A.; Zubkova, O. V.; Schramm, V. L.; Zheng, W.; Wolberger, C. Structural Insights into Intermediate Steps in the Sir2 Deacetylation Reaction. *Structure* **2008**, *16*, 1368-1377.

(2) Rostkowski, M,; Olsson, M. H.; Søndergaard, C. R.; Jensen, J. H. Graphical Analysis of pH-dependent Properties of Proteins Predicted Using PROPKA. *BMC Struct. Bio.* 2011, **11**:6.

(3) Darden, T.; York, D.; Pedersen, L. Particle Mesh Ewald - an N.Log(N) Method for Ewald Sums in Large Systems. *J. Chem. Phys.* **1993**, *98*, 10089-10092.

(4) Essmann, U.; Perera, L.; Berkowitz, M. L.; Darden, T.; Lee, H.; Pedersen, L. G. A Smooth Particle Mesh Ewald Method. *J. Chem. Phys.* **1995**, *103*, 8577-8593.

(5) Ryckaert, J. P.; Ciccotti, G.; Berendsen, H. J. C. Numerical Integration of the Cartesian Equations of Motion of a System with Constraints: Molecular Dynamics of n-Alkanes. *J. Comput. Phys.* **1977**, *23*, 327-341.

(6) Berendsen, H. J. C.; Postma, J. P. M.; Vangunsteren, W. F.; Dinola, A.; Haak, J. R. Molecular-Dynamics with Coupling to an External Bath. *J. Chem. Phys.* **1984**, *81*, 3684-3690.

(7) Case, D. A.; Darden, T. A.; Cheatham, III, T. E.; Simmerling, C. L.; Wang, J.; Duke, R. E.; Luo, R.; Crowley, M.; Walker, R. C.; Zhang, W.; et al. AMBER10, University of California, San Francisco: 2008.

(8) Cornell, W. D.; Cieplak, P.; Bayly, C. I.; Gould, I. R.; Merz, K. M.; Ferguson, D. M.; Spellmeyer, D. C.; Fox, T.; Caldwell, J. W.; Kollman, P. A. A 2nd Generation Force-field for the Simulation of Proteins, Nucleic-Acids, and Organic-Molecules. *J. Am. Chem. Soc.* **1995**, *117*, 5179-5197.

(9) Junmei, W.; Cieplak, P.; Kollman, P. A. How Well Does a Restrained Electrostatic Potential (RESP) Model Perform in Calculating Conformational Energies of Organic and Biological Molecules? *J. Comput. Chem.* **2000**, *21*, 1049-1074.

(10) Hornak, V.; Abel, R.; Okur, A.; Strockbine, B.; Roitberg, A.; Simmerling, C. How Well Does a Restrained Electrostatic Potential (RESP) Model Perform in Calculating Conformational Energies of Organic and Biological Molecules? *Proteins* **2006**, *65*, 712-725.

(11) Jorgensen, W. L.; Chandrasekhar, J.; Madura, J. D.; Impey, R. W.; Klein, M. L. Comparison of Simple Potential Functions for Simulating Liquid Water. *J. Chem. Phys.* **1983**, *79*, 926-935.

(12) Ryde, U. On the Role of Glu-68 in Alcohol Dehydrogenase. *Protein Sci.* **1995**, *4*, 1124-1132.

(13) Wang, J. M.; Wolf, R. M.; Caldwell, J. W.; Kollman, P. A.; Case, D. A. Development and Testing of a General Amber Force Field. *J. Comput. Chem.* **2004**, *25*, 1157-1174.

(14) Zhang, Y.; Lee, T.-S.; Yang, W. A Pseudobond Approach to Combining Quantum Mechanical and Molecular Mechanical Methods. *J. Chem. Phys.* **1999**, *110*, 46-54.

(15) Zhang, Y. Improved Pseudobonds for Combined Ab Initio Quantum Mechanical/Molecular Mechanical Methods. *J. Chem. Phys.* **2005**, *122*, 024114.

(16) Beeman, D. Some Multistep Methods for Use in Molecular-Dynamics Calculations. *J. Comput. Phys.* **1976**, *20*, 130-139.

(17) Shao, Y.; Fusti-Molnar, L.; Jung, Y.; Kussmann, J.; Ochsenfeld, C.; Brown, S. T.; Gilbert, A. T. B.; Slipchenko, L. V.;Levchenko, S. V.; O'Neill, D. P.; et al. Advances in Methods and Algorithms in a Modern Quantum Chemistry Program Package. *Phys. Chem. Chem. Phys.* **2006**, *8*, 3172-3191.

(18) Ponder, J. W. *TINKER, Software Tools for Molecular Design, version 4.2* **2004**.

(19) Zhang, Y.; Liu, H.; Yang, W. Free Energy Calculation on Enzyme Reactions with an Efficient Iterative Procedure to Determine Minimum Energy Paths on a Combined Ab Initio QM/MM Potential Energy Surface. *J. Chem. Phys.* **2000**, *112*, 3483.

(20) Souaille, M.; Roux, B. Extension to the Weighted Histogram Analysis Method: Combining Umbrella Sampling with Free Energy Calculations. *Comput. Phys. Commun.* **2001**, *135*, 40-57.

(21) Boczko, E. M.; Brooks, C. L. Constant-Temperature Free Energy Surfaces for Physical and Chemical Processes. *J. Phys. Chem.* **1993**, *97*, 4509-4513.

(22) Hu, P.; Wang, S.; Zhang, Y. How Do SET-domain Protein Lysine Methyltransferases Achieve the Methylation State Specificity? Revisited by Ab Initio QM/MM Molecular Dynamics Simulations. *J. Am. Chem. Soc.* **2008**, *130*, 3806-3813.

(23) Hu, P.; Wang, S.; Zhang, Y. Highly Dissociative and Concerted Mechanism for the Nicotinamide Cleavage Reaction in Sir2Tm Enzyme Suggested by Ab Initio QM/MM Molecular Dynamics Simulations. *J. Am. Chem. Soc.* **2008**, *130*, 16721-16728.
(24) Wu, R.; Wang, S.; Zhou, N.; Cao, Z.; Zhang, Y. A Proton-Shuttle Reaction Mechanism for Histone Deacetylase 8 and the Catalytic Role of Metal Ions. *J. Am. Chem. Soc.* **2010**, *132*, 9471-9479.
(25) Zhou, Y.; Wang, S.; Zhang,Y. Catalytic Reaction Mechanism of Acetylcholinesterase Determined by Born-Oppenheimer Ab Initio QM/MM Molecular Dynamics Simulations. *J. Phys. Chem. B* **2010**, *114*, 8817-8825.
(26) Ke, Z.; Guo, H.; Xie, D.; Wang, S.; Zhang, Y. Ab Initio QM/MM Free-Energy Studies of Arginine Deiminase Catalysis: The Protonation State of the Cys Nucleophile. *J. Phys. Chem. B* **2011**, *115*, 3725-3733.
(27) Ke, Z.; Smith, G. K.; Zhang, Y.; Guo, H. Molecular Mechanism for Eliminylation, a Newly Discovered Post-Translational Modification. *J. Am. Chem. Soc.* **2011**, *133*, 11103-11305.
(28) Zhou, Y.; Zhang, Y. Serine Protease Acylation Proceeds with a Subtle Re-Orientation of the Histidine Ring at the Tetrahedral Intermediate. *Chem. Commun.* **2011**, *47*, 1577-1579.
(29) Wu, R.; Lu, Z.; Cao, Z.; Zhang, Y. Zinc Chelation with Hydroxamate in Histone Deacetylases Modulated by Water Access to the linker Binding Channel. *J. Am. Chem. Soc.* **2011**, *133*, 6110-6113.
(30) Sauve, A. A.; Celic, I.; Avalos, J.; Deng, H. T.; Boeke, J. D.; Schramm, V. L. Chemistry of Gene Silencing: The Mechanism of NAD(+)-Dependent Deacetylation Reactions. *Biochemistry* **2001**, *40*, 15456-15463.
(31) Smith, B. C.; Denu, J. M. Sir2 Protein Deacetylases: Evidence for Chemical Intermediates and Functions of a Conserved Histidine. *Biochemistry* **2006**, *45*, 272-282.
(32) Hirsch, B. M.; Zheng, W. Sirtuin Mechanism and Inhibition: Explored with N(ε)-acetyl-lysine Analogs. *Mol. BioSyst.* **2011**, *7*, 16-28.